



**HAL**  
open science

## **Oxide Semiconductors: order within the disorder**

Elvira Fortunato, Luis Pereira, Pedro Barquinha, Isabel Ferreira,  
Rathinasamy Prabakaran, Goncalo Goncalves, Alexandra Goncalves, Rodrigo  
Ferrão Paiva Martins

► **To cite this version:**

Elvira Fortunato, Luis Pereira, Pedro Barquinha, Isabel Ferreira, Rathinasamy Prabakaran, et al..  
Oxide Semiconductors: order within the disorder. Philosophical Magazine, 2009, 89 (28-30), pp.2741-  
2758. 10.1080/14786430903022671 . hal-00519089

**HAL Id: hal-00519089**

**<https://hal.science/hal-00519089>**

Submitted on 18 Sep 2010

**HAL** is a multi-disciplinary open access archive for the deposit and dissemination of scientific research documents, whether they are published or not. The documents may come from teaching and research institutions in France or abroad, or from public or private research centers.

L'archive ouverte pluridisciplinaire **HAL**, est destinée au dépôt et à la diffusion de documents scientifiques de niveau recherche, publiés ou non, émanant des établissements d'enseignement et de recherche français ou étrangers, des laboratoires publics ou privés.



**Oxide Semiconductors: order within the disorder**

Journal:	<i>Philosophical Magazine &amp; Philosophical Magazine Letters</i>
Manuscript ID:	TPHM-09-Jan-0038.R1
Journal Selection:	Philosophical Magazine
Date Submitted by the Author:	06-Apr-2009
Complete List of Authors:	<p>Fortunato, Elvira; Materials Science Department, CENIMAT/I3N, Faculty of Science and Technology of New University of Lisbon and CEMOP/UNINOVA</p> <p>Pereira, Luis; Materials Science Department, CENIMAT/I3N, Faculty of Science and Technology of New University of Lisbon and CEMOP/UNINOVA</p> <p>Barquinha, Pedro; Materials Science Department, CENIMAT/I3N, Faculty of Science and Technology of New University of Lisbon and CEMOP/UNINOVA</p> <p>Ferreira, Isabel; Materials Science Department, CENIMAT/I3N, Faculty of Science and Technology of New University of Lisbon and CEMOP/UNINOVA</p> <p>Prabakaran, Rathinasamy; Materials Science Department, CENIMAT/I3N, Faculty of Science and Technology of New University of Lisbon and CEMOP/UNINOVA</p> <p>Goncalves, Goncalo; Materials Science Department, CENIMAT/I3N, Faculty of Science and Technology of New University of Lisbon and CEMOP/UNINOVA</p> <p>Goncalves, Alexandra; Materials Science Department, CENIMAT/I3N, Faculty of Science and Technology of New University of Lisbon and CEMOP/UNINOVA</p> <p>Martins, Rodrigo; Materials Science Department, CENIMAT/I3N, Faculty of Science and Technology of New University of Lisbon and CEMOP/UNINOVA</p>
Keywords:	oxide thin films, solar cells, thin-film transistors
Keywords (user supplied):	ordered and disordered semiconductors, solar cells

1  
2  
3  
4  
5  
6  
7  
8  
9  
10  
11  
12  
13  
14  
15  
16  
17  
18  
19  
20  
21  
22  
23  
24  
25  
26  
27  
28  
29  
30  
31  
32  
33  
34  
35  
36  
37  
38  
39  
40  
41  
42  
43  
44  
45  
46  
47  
48  
49  
50  
51  
52  
53  
54  
55  
56  
57  
58  
59  
60



For Peer Review Only

## Oxide Semiconductors: order within the disorder

E. Fortunato, L. Pereira, P. Barquinha, I. Ferreira, R. Prabakaran, G. Gonçalves, A. Gonçalves, R.

Martins

Materials Science Department, CENIMAT/I3N, Faculty of Science and Technology of New University of Lisbon and CEMOP/UNINOVA, Campus de Caparica, 2829-516 Caparica, Portugal

### ABSTRACT

This paper discusses the effect of order and disorder on the electrical and optical performance of ionic oxide semiconductors used to produce optoelectronic devices such as pn heterojunction solar cells and thin-film transistors. The obtained results show p-type c-Si/a-IZO/poly-ZGO solar cells exhibiting efficiencies above 14% in device areas of about 2.34 cm<sup>2</sup> while amorphous oxide TFTs based on the Ga-Zn-Sn-O system demonstrate superior performance than the polycrystalline ZnO TFTs, with  $I_{ON}/I_{OFF}$  ratio exceeding  $10^7$ , turn-on voltage below 1-2 V and saturation mobility above 25 cm<sup>2</sup>/Vs. Apart from that, preliminary data on p-type oxide TFT based on the Zn-Cu-O system will also be presented.

**Keywords:** oxide semiconductors, thin film transistors; ordered and disordered semiconductors; solar cells.

### 1. Introduction

N-type oxide semiconductors have been extensively used as transparent conductive electrodes for display and solar cells applications[1-3] where the most used oxides are based on indium tin oxide alloys (ITO), due to their high transmittance in the visible range of the solar spectrum and the low

1  
2  
3 sheet resistance [4-7]. Due to cost increase of indium and the need to have films able to sustain a  
4  
5 hydrogen plasma discharge during the deposition process [8], zinc aluminum oxide (ZAO) [9-13]  
6  
7 and zinc gallium oxide (ZGO) have been developed as a promising alternative to ITO, since zinc  
8  
9 (Zn) is a quite abundant (about  $10^3$  more than In [14]) and “green” material. Besides that, gallium  
10  
11 (Ga) has a better doping efficiency than aluminum (Al), allowing room temperature processing [12,  
12  
13 15, 16]. For these films, the conductivity improvement has been associated with the crystal order  
14  
15 and corresponding grain size. Recently, it has also been realized that disordered oxide  
16  
17 semiconductors can present excellent optical and electrical properties, namely high conductivity and  
18  
19 high mobility, even when processed at room temperature, compatible with the use of flexible  
20  
21 substrates [17, 18].  
22  
23  
24  
25  
26

27  
28 The use of n-type oxide semiconductors in active electronic functions has been also demonstrated in  
29  
30 the last 5-8 years [19-21], even when produced at room temperature [22, 23], which extends their  
31  
32 ability to be processed on other type of substrates, such as paper [24-28]. Nowadays these active  
33  
34 oxides are key components in a wide range of device applications like sensors [29] and thin-film  
35  
36 transistors (TFTs), where it has been demonstrated that they can present high electronic  
37  
38 performance even when disordered ionic oxides are used [30-36]. Concerning p-type oxide  
39  
40 semiconductors, this activity has been also pursued in the last years [37-45]. Recently, a p-type TFT  
41  
42 based on low band gap SnO has been reported [46], in spite of the difficulty in having metals with a  
43  
44 high work function, that are able to perform the required ohmic contact with the p-type oxide with a  
45  
46 low carrier concentration (below  $10^{16}$  carriers/cm<sup>3</sup>) [3, 47].  
47  
48  
49  
50

51  
52 When comparing the electronic performance of the oxides above mentioned with the covalent  
53  
54 semiconductors, we observe huge differences, either concerning the doping effect or the role of  
55  
56 disorder and order on the materials and devices' properties [48, 49]. In fact, in covalent  
57  
58 semiconductors, the electronic doping effect is mainly related to the substitution of atoms in a  
59  
60 matrix (host) by an impurity, which may have a deficit or an excess of valence electrons relatively

1  
2  
3 to the host atoms, leading to a negative or positive charge impurity, to each is connected the  
4  
5 existence of an excess of free holes (p-type), or of free electrons (n-type), respectively [50]. The n-  
6  
7 doping effect in oxide semiconductors is essentially related to the existence of oxygen vacancies  
8  
9 (meaning that the films are non stoichiometric and so there are not enough anions to compensate the  
10  
11 existing cations), which work as a source for electrons. Their control depends on the oxidation state  
12  
13 of the cation, which leads to changes in the film composition, as opposed to the substitutional  
14  
15 doping in covalent semiconductors [18, 29]. For p-type oxides, a passivation of vacancies and deep  
16  
17 defects is also necessary prior to the introduction of the correct impurities in the host matrix [39]. In  
18  
19 covalent semiconductors disorder leads to a continuous distribution of localized states, between the  
20  
21 edges of the conduction and valence bands. This leads to a strong decrease (several orders of  
22  
23 magnitude) of the carriers' mobility [51]. For oxides based in heavy metal cations, this is not the  
24  
25 case. Disorder does not lead to the existence of a full carrier's localization and so carrier's mobility  
26  
27 is not strongly affected, as it happens in covalent semiconductors [52-54]. This is translated by a  
28  
29 clear superiority of these materials when used for applications such as thin film transistors, TFT,  
30  
31 [51], whose become popular after the report on the feasibility of doping amorphous silicon (a-Si:H)  
32  
33 by the glow discharge technique [55], followed by the production in 1979 of the first TFT by  
34  
35 LeComber, Spear and Ghaith, using a-Si:H as the active semiconductor material [56]. Although this  
36  
37 result attract much attention of the display industry, the major disadvantage of a-Si:H TFT is its low  
38  
39 electron mobility that limits the ultimate speed of devices. However, an adequate device speed for  
40  
41 the switching applications in the LCD has been achieved [57]. Since the mid-1980s the silicon-  
42  
43 based thin film transistors become the most important devices for active matrix liquid crystal  
44  
45 displays (AMLCDs), and have successful dominated the large area LCD product market [58]. The  
46  
47 emerging of the novel oxide active semiconductors [59] and the production of the first ZnO TFT at  
48  
49 room temperature [23] opened new prospects concerning the use of low cost flexible and disposable  
50  
51 substrates, such as paper [25], opening so a new era of electronic devices away from the silicon.  
52  
53  
54  
55  
56  
57  
58  
59  
60

1  
2  
3 In this paper we report on the optical and electrical performance of materials and devices based on  
4 ordered and disordered Zinc Oxide (ZnO) and Zinc Gallium Oxide (ZGO), without and with tin  
5 (Sn) in its composition (ZGSO). Besides that, a first attempt to produce a p-type TFT based on wide  
6 band gap oxide semiconductors will also be reported.  
7  
8  
9  
10  
11

## 12 13 14 **2. Experimental details**

15  
16 The ZnO, ZGO and ZGSO films were produced by rf magnetron sputtering using a single 3 inches  
17 diameter ZnO or ZnO:Ga<sub>2</sub>O<sub>3</sub> (95:5 wt%) ceramic target or by co-sputtering, using the ZnO:Ga<sub>2</sub>O<sub>3</sub>  
18 target and a 2 inches diameter Sn target, (see fig. 1) always with a base pressure below  $3 \times 10^{-4}$  Pa.  
19  
20 Other deposition parameters were adjusted as described elsewhere [15, 60].  
21  
22  
23  
24  
25

26 To produce the pn heterojunction solar cells, doped p-type crystalline silicon substrates (p-type c-Si,  
27 2.5×2.5 cm in size), 150 μm thick and with an acceptor concentration in the range of  $5-10 \times 10^{16}$   
28  $\text{at.cm}^{-3}$  were used. The polished surfaces of the crystalline silicon substrate were cleaned (etching  
29 the native oxide with a buffered HF solution) and properly rinsed prior to the deposition of the back  
30 metal contact by e-beam evaporation, composed by a double layer of silver and chromium (Ag/Cr),  
31 200 nm thick. The n-type polycrystalline ZGO, 100-200 nm thick, was deposited at room  
32 temperature (R.T.) by r.f. magnetron sputtering on the opposite side of the substrate, showing a  
33 resistivity ( $\rho$ ) below  $7 \times 10^{-4}$  Ω.cm. In selected devices, a 5-10 nm n-type interlayer based on  
34 amorphous indium zinc oxide (a-IZO) with a resistivity in the range of  $7-1 \times 10^{-4}$  Ω.cm was  
35 deposited, using the conditions described elsewhere [61, 62]. The front metal grid contact was  
36 based on Cr/Ag, also deposited by e-beam evaporation. The entire device (with or without the front  
37 metal electrode) was annealed in N<sub>2</sub>/H<sub>2</sub> (95/5) atmosphere for 30 minutes at 150 and 250 °C,  
38 respectively.  
39  
40  
41  
42  
43  
44  
45  
46  
47  
48  
49  
50  
51  
52  
53  
54  
55  
56

57 The ZnO and ZGSO bottom-gate n-type TFTs were produced using heavily doped p-type c-Si  
58 substrates coated with 100 nm thick thermally grown SiO<sub>2</sub>, which acts as the gate dielectric, leading  
59 to a gate leakage current ( $I_G$ ) below 10 pA for all the produced devices. Si was simultaneously used  
60

1  
2  
3 as the substrate and the common gate of the devices. A 5/75 nm thick Ti/Au film was deposited by  
4  
5 e-beam evaporation on the backside of Si (after etching the backside SiO<sub>2</sub> with a buffered HF  
6  
7 solution) to form the gate electrode. A 30-60 nm thick polycrystalline ZnO or amorphous ZGSO (a-  
8  
9 ZGSO) layer (the semiconductor) was then deposited by r.f. magnetron sputtering in an Ar/O<sub>2</sub>  
10  
11 atmosphere. In the co-sputtering case, the rf power density ratio applied to the ZGO and to the Sn  
12  
13 targets was kept around 1.7. The 200 nm thick source/drain electrodes (Ti) were e-beam evaporated  
14  
15 at a rate of 2 Å/s on top of ZnO or a-ZGSO. Both the semiconductor and the source/drain layers  
16  
17 were patterned by lift-off and the produced transistors had a fixed width (W) of 50 μm and length  
18  
19 (L) of 50 μm. Two different series of a-ZGSO transistors, S1 and S2, were produced: in S1, the a-  
20  
21 ZGSO was produced at room temperature, while in S2 it was deposited at 150 °C. After production,  
22  
23 both series of TFTs were annealed in a Barnstead Thermolyne F21130 tubular furnace, with a  
24  
25 constant flow of nitrogen, at 150, 200, 250 and 300 °C for 1 hour. The first attempts to produce p-  
26  
27 type TFT involved the co-sputtering of ZnO and Cu (ZCO) at 150 °C, using an rf power ratio  
28  
29 between targets of 1.2. After processing, the films were annealed up to 350°C. The other procedures  
30  
31 were similar to the ones already described for the ZnO and ZGSO TFT.  
32  
33  
34  
35  
36  
37  
38

39 The films' thicknesses were measured with a surface profilometer Sloan Tech Dektak 3. X-ray  
40  
41 diffraction measurements were performed at RT in air, using the CuKα line (λ=1.5418 Å) of a  
42  
43 Siemens D-500 diffractometer. The scanning electron microscopy (SEM) analysis was done in a  
44  
45 FEI Strata 235-Dual Beam FIB (both in surface and cross section after vertical milling using Ga  
46  
47 ions). Atomic force microscopy (AFM) images were also taken for the same set of films, using an  
48  
49 Asylum AFM. X-ray Photoelectron Spectroscopy (XPS) analysis was performed using the Al Kα  
50  
51 (non monochromatic) radiation of an XSAM800 (KRATOS) spectrometer operated in the fixed  
52  
53 analyzer transmission (FAT) with a power of 120 W (10 mA and 12 kV) in order to evaluate the  
54  
55 composition and chemical states of the produced oxide thin films, as well as their chemical  
56  
57 composition. Spectra acquisition was done without flood gun, the carbonaceous contamination (C  
58  
59  
60

1  
2  
3 1s binding Energy = 285 eV) being used as reference for binding energy correction. For quantitative  
4 data treatment, sensitivity factors provided by the equipment manufacturer were used.  
5  
6

7  
8 The optical characteristics of the films were measured using a UV-VIS-IR spectrophotometer (3100  
9 Shimadzu double beam) and a Jobin-Yvon UVISEL ellipsometer in the spectral range from 0.65 to  
10 6.5 eV at an incidence angle of 70°. To determine the optical parameters of the films under analysis,  
11 we used a Tauc-Lorentz dispersion model with two oscillators. The electrical and optical properties  
12 of the oxide films produced were evaluated in 150-200 nm thick films, deposited on Corning 1737  
13 glass substrates. The Ti/Au electrode patterns were obtained using shadow masks and their  
14 geometries are shown in the sketch of fig 1.c), for conductivity versus temperature (top) and Hall  
15 effect (bottom) measurements.  
16  
17

18 The I-V curves of the pn solar cells (Ag-Cr/p-c-Si/a-IZO/p-ZGO/Ag-Cr) were performed in the  
19 dark and under AM1.5 illumination using a Spire sun simulator. The electrical characterization of  
20 the transistors was performed using an Agilent 4155C semiconductor parameter analyzer and a  
21 Cascade Microtech M150 probe station. All the analyses were performed with a relative humidity  
22 of 35-40% and inside a dark box.  
23  
24  
25  
26  
27

### 28 **3. Results**

#### 29 **3.1 Material properties**

30 Before selecting the films for device fabrication, their structure, morphology and electro-optical  
31 characteristics were studied and related to the selected deposition parameters. Figure 2 shows the  
32 XRD patterns of the a-IZO, poly-ZnO and poly-ZGO films deposited on Corning substrates (center)  
33 and the corresponding surface morphology images obtained by AFM (left side) and SEM (right  
34 side). These films were used to fabricate the pn heterojunction solar cells and the poly-ZnO TFT.  
35 Figure 3 shows the XRD patterns (a), the SEM surface (c) and AFM (d) images of the ZGSO films  
36 used as semiconductor in TFTs. A SEM cross section (b and e) is also shown for two device  
37 structures (p-c-Si/SiO<sub>2</sub>/a-ZGSO and p-c-Si/a-IZO/ZGO) used to fabricate TFTs and solar cells,  
38  
39  
40  
41  
42  
43  
44  
45  
46  
47  
48  
49  
50  
51  
52  
53  
54  
55  
56  
57  
58  
59  
60

1  
2  
3 respectively. The composition of the ZGSO films was analyzed by XPS, for films that have  
4  
5 sustained different annealing temperatures. The results achieved are depicted in Table 1.  
6  
7

8  
9 The degree of films compactness and nature of the films structure were also analyzed by  
10  
11 spectroscopic ellipsometry aiming to compare the behavior of the ZGO and ZGSO films. The  
12  
13 results are depicted in fig.4 a) for the refractive index (n) and the extinction coefficient (k) as a  
14  
15 function of the photon energy [54].  
16  
17

18  
19 As far as the visible transmittance is concerned, all films exhibit values above 75%, with the highest  
20  
21 ones for the IZO films (87%). Also the optical band gap inferred from transmittance and  
22  
23 spectroscopic ellipsometry data reveal that all films have an optical band gap above 3 eV.  
24  
25

26  
27 The electrical properties of the films were also studied through the conductivity versus temperature  
28  
29 and the Hall effect measurements. All films with  $\rho < 10^{-3} \Omega \cdot \text{cm}$  are non-activated, as expected for  
30  
31 degenerated oxide semiconductors [3]. For highly resistive films ( $\rho > 10^{10} \Omega \cdot \text{cm}$ ), we could not  
32  
33 determine the activation energy through the conductivity measurements, while for the so-called  
34  
35 active oxide semiconductors (either polycrystalline or amorphous) this was accomplished, as shown  
36  
37 for example in fig. 4b) for 300 °C annealed a-ZGSO films.  
38  
39

40  
41 Table 2 also shows the Hall Effect data of the ZnO, ZGO and ZGSO films used for the devices  
42  
43 fabricated and studied along this work. There, we refer to the performance of films processed in  
44  
45 different conditions: the ones grown above the Sn target are richer in Sn than the ones located close  
46  
47 to the ZGO target (see fig.1).  
48  
49

### 50 51 **3.2 Solar cells**

52

53  
54 The I-V curves of the p-c-Si/poly-ZGO and p-c-Si/a-IZO/poly-ZGO solar cells taken under AM1.5  
55  
56 illumination are depicted in fig. 5 as curves (a) and (b), respectively. The corresponding  
57  
58 performance of the devices analyzed under AM1.5 illumination conditions are shown in Table 3.  
59  
60

### 3.3 *N-type thin film transistors*

The transfer and output characteristics of the n-type ZnO and a-ZGSO TFTs are depicted in fig. 6, for films processed in the central region of the sputtering system (see fig. 1), at R.T. (ZnO) and 150°C (a-ZGSO S2). With a low temperature annealing (150 °C) the ZnO TFTs already present nice properties despite the low saturation mobility ( $\mu_{SAT}$ ), slightly higher than 1 cm<sup>2</sup>/Vs.  $\mu_{SAT}$  is enhanced by annealing at 300 °C, however all the remaining properties are degraded (fig. 4 a and b). Concerning the a-ZGSO based devices (fig. 6 c and d), channel conductivity modulation is negligible until the devices are annealed above 200 °C, and the properties are even improved at 300 °C.

The electrical characteristics of the ZnO and a-ZGSO TFTs deposited at RT (S1) and 150 °C (S2) and annealed up to 300 °C are shown in Table 4.

### 3.4 *p-type thin film transistors*

The transfer and output characteristics of the p-type TFT based on the Zn-Cu-O system (ZCO) after being annealed at 350 °C are depicted in fig. 7. From the data depicted we take On/Off ratios of about 10<sup>2</sup>, with saturation mobilities below 9×10<sup>-2</sup> cm<sup>2</sup>V<sup>-1</sup>s<sup>-1</sup>.

## 4. Discussion of the results

### 4.1 *Materials*

Figures 2 and 3 show the structure and surface morphology of the IZO, ZGO and ZGSO films processed at room temperature. The data depicted show that the IZO films are amorphous exhibiting a smooth surface, with Rms roughness below 0.5 nm. The film structure does not change after annealing at 250 °C. On the other hand, the ZGO films are polycrystalline with a preferred (0002) grain orientation and a roughness above 15-18 nm that is enhanced as the annealing temperature increases. This behavior is ascribed to the increase of the crystalline size [15]. Similar results were found for ZnO. The XRD patterns (as produced and after being annealed at 300°C in a

1  
2  
3 nitrogen atmosphere), AFM and SEM images reveal that the ZGSO films are amorphous, with a  
4 surface Rms roughness below 0.7 nm.  
5  
6

7  
8 Figure 4a) shows the refractive index and the extinction coefficient spectra for the poly-ZGO and a-  
9 ZGSO thin films depicted in fig. 2. The data show that near the band gap energy (3.6 eV) the poly-  
10 ZGO thin film exhibits a sharp peak associated to an abrupt variation of the extinction coefficient,  
11 which is attributed to the crystalline nature of the films, in-line with the XRD data. On the other  
12 hand, the spectra of the a-ZGSO films exhibit a broad band whose peak is shifted to higher  
13 energies. This type of behavior is typical of amorphous structures [63-67]. By comparing both  
14 films, the poly-ZGO has a higher refractive index in the transparent region than the a-ZGSO.  
15 Concerning the extinction coefficients, the a-ZGSO films present threshold energy higher than that  
16 of poly-ZGO. These results have also been observed for the case of a-GIZO thin films [68].  
17  
18

19  
20 In spite of the films' structure and morphology data do not show any detectable variation after  
21 annealing at 300 °C, the same does not occur to the electrical properties, especially for the a-ZGSO  
22 films, as can be seen in Table 2. The data reveal that as deposited (R.T.) poly-ZGO films are highly  
23 conductive ( $\rho \approx 10^{-4} \Omega \cdot \text{cm}$ ), as desirable for applications as transparent conductive oxides. The same  
24 does not happen with the poly-ZnO and a-ZGSO films (rich or not in Sn), deposited at RT which  
25 are highly resistive (respectively higher than  $10^5 \Omega \cdot \text{cm}$  and  $10^{10} \Omega \cdot \text{cm}$ ). However, after annealing to  
26 300 °C, the resistivity decreases by more than 3 order and 8 orders of magnitude, respectively for  
27 the poly-ZnO and a-ZGSO films. Besides that, after annealing the a-ZGSO films are activated, as  
28 shown by the Arrhenius plot in fig. 4b). The data show that the conductivity of Sn richer a-ZGSO  
29 films present an activation energy of 0.14 eV, while the ones with the lower Sn content exhibit an  
30 activation energy of 0.19 eV.  
31  
32

33  
34 The decrease in resistivity with the annealing temperature is attributed to modification of the  
35 semiconductor and/or to the improved local atomic rearrangement, possibly related to a change in  
36 the oxidation state of Sn, from  $\text{Sn}_4^+$  to  $\text{Sn}_2^+$ . It is well known that  $\text{Sn}_2^+$  absorbs at an energy range  
37  
38  
39  
40  
41  
42  
43  
44  
45  
46  
47  
48  
49  
50  
51  
52  
53  
54  
55  
56  
57  
58  
59  
60

1  
2  
3 lower than  $\text{Sn}_4^+$ , which explains the lower absorption coefficient observed for annealed a-ZGSO  
4 samples, as observed by Hosono et al [69] in optical measurements performed to evaluate the  
5 behavior of the absorption coefficient in a-ZGSO films. With increasing annealing temperature,  
6 there is a surface enrichment in Ga and especially in Sn.  
7  
8  
9

10 This interpretation is reinforced by the XPS data shown in Table 1, for a-ZGSO films annealed up  
11 to 300 °C. The data show that as the annealing temperature increases up to 300 °C, the films'  
12 stoichiometry changes. The most noticeable changes are related to oxygen associated to oxide metal  
13 elements (which increases about 28.2%) or to hydroxide groups (which decreases about 39.4%).  
14 That is, ratio O(oxide)/O(hydroxide) increases with the annealing temperature, which could be  
15 related to oxygen adsorption from the environment and hydroxide groups. The Ga/Zn and Sn/Zn  
16 atomic ratio in as-deposited and 300 °C annealed samples reveal an enhancement of about 71.4%  
17 and 107.4%, respectively. These data clearly show that Sn changes its state of oxidation with the  
18 annealing process, leading to changes in the films' stoichiometry, involving Sn segregation towards  
19 the surface, with or without cations redistribution along the a-ZGSO thickness. Regarding  
20 photoelectron binding energy (B.E.) of different elements, they correspond to the oxidized forms  
21 B.E.(Ga 2p)= $1118.7 \pm 0.2$  eV, typical of Ga 2p from  $\text{Ga}_2\text{O}_3$  [70] and B.E.(Zn 2p)= $1022.3 \pm 0.2$  eV,  
22 typical of Zn 2p from ZnO (see. NIST X-ray Photoelectron Spectroscopy Database,  
23 <http://srdata.nist.gov/xps/>, 2003). Concerning Sn, its photoelectrons Sn 3p and Sn 3d are present in  
24 all the samples, corresponding to binding energies of  $716.1 \pm 0.2$  and  $486.2 \pm 0.2$  eV, respectively.  
25 This can be assigned either to SnO or  $\text{SnO}_2$ , due to their binding energy proximity and the  
26 dispersion of values in literature. A more robust parameter, independent of charge accumulation  
27 correction, is the modified Auger parameter which is, for all the samples,  $918.3 \pm 0.2$  eV which is  
28 closer to the  $\text{SnO}_2$  modified Auger parameter than to the SnO one [71]. O 1s peak is fitted with two  
29 components centered at  $530.4 \pm 0.2$  eV and at  $532.1 \pm 0.2$  eV assignable, respectively to the oxide  
30 and hydroxide oxygen forms.  
31  
32  
33  
34  
35  
36  
37  
38  
39  
40  
41  
42  
43  
44  
45  
46  
47  
48  
49  
50  
51  
52  
53  
54  
55  
56  
57  
58  
59  
60

1  
2  
3 Another indirect result from XPS data concerns spectra charge shifts which were 9.5 eV, 8.5 eV and  
4 4 eV for RT, 200 °C and 300 ° C, respectively. This is an indication that the number of hole traps in  
5  
6 the samples decrease with the annealing temperature. These results are directly related with the  
7  
8 electrical properties exhibited by these films, where a tremendous improvement was observed,  
9  
10 mainly for the carrier concentration.  
11  
12  
13

#### 14 15 16 **4.2 Solar cells**

17  
18 Growing a ZGO film on silicon to form a heterojunction is potentially attractive for PV applications  
19  
20 because such cells can have an excellent blue response (in contrast to many industrial c-Si solar  
21  
22 cells which feature a heavily doped “dead” layer at the illuminated surface) and can be fabricated in  
23  
24 a relatively simple way. The ITO/c-Si structure has been extensively studied during the past two  
25  
26 decades by various deposition technologies. The conversion efficiencies achieved were 10-15%  
27  
28 using spray pyrolysis [72], 9.8% using electron beam evaporation [73], and 12-16.5% using ion-  
29  
30 beam sputtering [74]. However, little information is available in the literature on ZnO/c-Si  
31  
32 heterojunction solar cells [75], and all the cells reported until now have a low energy conversion  
33  
34 efficiency. In fig. 5 we present the electrical I-V curves under AM1.5 illumination of p-type c-Si/n-  
35  
36 type poly-ZGO and p-type c-Si/a-IZO/n-type poly-ZGO heterojunction solar cells in a total active  
37  
38 area of about 2 cm<sup>2</sup>. The device without the a-IZO under layer (fig. 5a)) presents short circuit  
39  
40 current density ( $J_{SC}$ ), open circuit voltage ( $V_{OC}$ ), fill factor (FF) and conversion efficiency ( $\eta$ ) of  
41  
42 31.15 mAcm<sup>-2</sup>, 488.8 mV, 0.59 and 9 %, respectively. For the device with the underneath a-IZO n-  
43  
44 type layer (fig. 5b)) with a thickness below 10 nm, a work function above 4.85 eV and whose  
45  
46 electronic carrier mobility measured by Hall effect is above 60 cm<sup>2</sup>V<sup>-1</sup>s<sup>-1</sup>, the obtained properties  
47  
48 are:  $J_{SC} = 31.88$  mAcm<sup>-2</sup>;  $V_{OC} = 558.8$  mV; FF = 0.79;  $\eta = 14.09$  %. The data show an overall  
49  
50 improvement on the solar cell performance above 56.6 % when the a-IZO intermediate layer is  
51  
52 used. The most optimized device parameter is the FF (>33 %), followed by the  $V_{OC}$  (>14 %).  
53  
54  
55  
56  
57  
58  
59  
60

1  
2  
3 This improvement could be related to a better matching promoted at the interface between the n-  
4 type poly-ZGO oxide and the p-type c-Si by the a-IZO, due to its work function and because the  
5 highly smooth surface of a-IZO films reduces the leakage current related to pinholes formation.  
6  
7  
8  
9  
10 Indeed, due to the electronic performance of the thin IZO interlayer it governs the improved  $V_{oc}$   
11 while the rest of the TCO layer serves largely to provide proper anti reflecting coating and lateral  
12 conduction properties. This leads to an improvement of the shunt and series resistances of the  
13 device and to a better collection efficiency. No degradation of the cell efficiency was observed  
14 during a 50-hour illumination test (1 sun) and after storing the cell in air for six months.  
15  
16  
17  
18  
19  
20  
21

### 22 **4.3 N-type thin film transistors**

23  
24  
25 Figure 6 and Table 4 show the transfer and output characteristics as well as the extracted electrical  
26 parameters of the n-type oxide TFTs analyzed in this work. In general, the data show that the  
27 performance of the amorphous TFTs is far better than the one of the poly-ZnO based devices.  
28 Besides that, the annealing treatment leads to electrical improvements on the amorphous oxide  
29 TFTs while the same does not occur to the polycrystalline oxide TFTs. Table 3 shows the results of  
30 a-ZGSO produced at R.T. (S1) and 150 °C (S2), before and after annealing. Note that for both  
31 series of a-ZGSO TFTs the non-annealed devices do not work properly, having always very low  $I_D$   
32 even for  $V_G=40$  V or 50 V and hence small channel conductivity modulation, being this even more  
33 significant for the S1 series. In fact, with the processing conditions used in this work, for maximum  
34 temperatures of 150 °C the best performance was obtained with poly-ZnO instead of a-ZGSO  
35 transistors.  
36  
37  
38  
39  
40  
41  
42  
43  
44  
45  
46  
47  
48  
49  
50

51  
52 The data in Table 4 show that the a-ZGSO TFT of S1 series start working properly only for  
53 annealing temperatures higher than 250 °C, while for the S2 TFT series, even though they work  
54 before annealing, the electrical behavior is not stable: for successive and repeated measurements a  
55 significant positive turn-on voltage ( $V_{on}$ ) shift [30] higher than 15 V is observed, which should be  
56 related with electron trapping close to the insulator-semiconductor interface. Only after annealing at  
57  
58  
59  
60

1  
2  
3 200 °C the S2 TFT series present stable and reproducible electrical characteristics. Concerning  $\mu_{SAT}$   
4 (calculated by the derivative of the  $\sqrt{I_D}(V_G)$  plot with  $V_D=20$  V) an increase is observed with the  
5  
6 annealing temperature for both series of TFTs analyzed, with a maximum value in the order of 25  
7  
8  $cm^2/Vs$ , for a-ZGSO films processed with an initial temperature of 150 °C (S2). This improvement  
9  
10 with annealing temperature is attributed to modification of the semiconductor/insulator interface  
11  
12 with temperature and/or to improved local atomic rearrangement [76] as it was confirmed by the  
13  
14 XPS analysis. The threshold voltage ( $V_T$ ) is generally lower for S2 than for S1 devices, around 5  
15  
16 and 6.5 V respectively, showing a trend to decrease as the annealing temperature increases. Again,  
17  
18 this should be related with improved film and interface properties (for instance, lower density of  
19  
20 traps or better atomic rearrangement, as already suggested above) when a-ZGSO is produced or  
21  
22 annealed at higher temperatures. The  $I_{ON}/I_{OFF}$  ratio for both series of a-ZGSO TFTs is around  $10^7$ -  
23  
24  $10^8$ , which is around 1 order of magnitude higher than the one obtained for the poly-ZnO TFTs. As  
25  
26 can be seen from fig. 6, this difference is essentially related with differences in  $I_{ON}$ , since  $I_{OFF}$  is  
27  
28 controlled by the  $SiO_2$  leakage current.  
29  
30  
31  
32  
33  
34  
35

36  
37 Another significant difference between the presented poly-ZnO and a-ZGSO devices is the  
38  
39 evolution of their  $\mu_{SAT}$  values with  $V_G$ . For poly-ZnO, it can be seen that there is a trend to a  
40  
41 continuous increase of  $\mu_{SAT}$  while for a-ZGSO it saturates and starts to decrease for higher values of  
42  
43  $V_G$  (fig. 6 a) and c)). The trend verified for ZGSO is also typically found for a-GIZO or other  
44  
45 amorphous oxide semiconductors, being the decrease for higher  $V_G$  associated with the higher  
46  
47 scattering that the electrons are subjected to as they move closer to the dielectric/semiconductor  
48  
49 interface, which is reinforced by the higher scattering associated with the high  $V_D$  used (generally,  
50  
51 for devices without contact problems,  $\mu_{FE} > \mu_{SAT}$ ) [30]. Nevertheless, even if not presented in fig. 6  
52  
53 a), in poly-ZnO TFTs the same  $\mu_{SAT}$  evolution is visible if  $V_G$  is taken to higher values, like 80 V.  
54  
55 Until  $V_G=30$  V poly-ZnO TFT  $\mu_{SAT}$  always increases due to the preponderance of the modulation of  
56  
57 grain boundaries associated barriers as  $V_G$  increases, when compared to the scattering phenomena  
58  
59  
60

described above. Also due to these grain boundaries and to the higher roughness of poly-ZnO films, the maximum  $\mu_{\text{SAT}}$  is considerably lower than the one obtained for a-ZGSO TFTs.

Besides the worst interface properties of  $\text{SiO}_2/\text{ZnO}$ , the higher values of subthreshold voltage swing (S) verified for poly-ZnO TFT can also be related with the presence of the grain boundaries barriers, which inhibit carrier transport, as opposed to the percolation conduction of the a-ZGSO through overlapping *s* orbitals. Besides that, S values are lower for 150 °C than R.T. produced a-ZGSO TFTs, which is again supported by the better interface and local atomic rearrangement of the films produced at higher temperature.

#### 4.4 P-type thin film transistors

In fig. 7 we depict the preliminary electrical characteristics of p-type ZCO TFTs. The data reveal devices with  $I_{\text{ON}}/I_{\text{OFF}}$  ratio of about  $10^2$ ,  $V_{\text{on}} \cong -21$  V and  $\mu_{\text{SAT}} \approx 0.09 \text{ cm}^2 \text{ V}^{-1} \text{ s}^{-1}$ . The observed behavior is attributed to the change of Cu oxidation state (from  $\text{Cu}^+$  to  $\text{Cu}^{2+}$ ) [77], with some possible surface state passivation induced by  $\text{N}_2$ , after annealing the device in a  $\text{N}_2$  atmosphere at 350 °C. This is still an open discussion that requires further work, aiming for a better understanding of the device behavior and the overall improvement of the electrical characteristics achieved.

## 5. Conclusions

In summary, we have demonstrated the possibility to produce high performance oxide based pn heterojunction solar cells and bottom gate TFTs using ordered and disordered semiconductors. Poly-ZGO proves to be an excellent candidate to fabricate solar cells with high efficiencies at very low cost, when compared to the traditional technologies. We observed a tremendous gain on the solar cell performance when an intermediate a-IZO layer is used between the p-type c-Si and the n-type poly-ZGO. The obtained solar cell characteristics are remarkable, specially the efficiency, which can be as high as 14 % in the entire active device area of  $2.34 \text{ cm}^2$ , opening so an area of research where we expect to improve by the present results.

1  
2  
3 As far as the bottom gate poly-ZnO and a-ZGSO TFT are concerned, we observed a considerable  
4  
5 improvement in the properties of devices based on a disordered channel layer material, after  
6  
7 annealing up to 300 °C. The data show that the annealing treatment dominates device characteristics  
8  
9 and minimizes the effect of other process parameters. The performance of the presented a-ZGSO  
10  
11 TFT is comparable and in some cases superior to those of a-GIZO TFTs that have been proved to  
12  
13 build up quite large area active matrix with excellent performances, when compared with today's  
14  
15 technology [33, 78]. This is a clear advantage since the replacement of In by Sn in the Ga-Zn-O  
16  
17 system, is quite important due to the limited availability of In. Apart from that, we also  
18  
19 demonstrated the possibility to produce a p-type oxide TFT using the Zn-Cu-O system, whose  
20  
21 results are quite encouraging for further activity.  
22  
23  
24  
25  
26  
27  
28

### 29 **Acknowledgements**

30  
31  
32 This paper was made in honour of Professor Walter Spear and his strong contribution to the field of  
33  
34 amorphous semiconductors, with emphasis to amorphous silicon and their alloys, and their  
35  
36 integration into devices. This work was funded by the Portuguese Science Foundation (FCT-  
37  
38 MCTES) through projects PTDC/CTM/23943/2006, PTDC/EEA-ELC/64975/2006. The authors  
39  
40 would also like to thank Portuguese Science Foundation (FCT-MCTES) for the fellowships  
41  
42 SFRH/BD/17970/2004 and SFRH/BD/27313/2006 given to two of the authors (Pedro Barquinha  
43  
44 and Gonçalo Gonçalves). Thanks are also due to Ana M. Botelho do Rego from IST (Portugal) and  
45  
46 Anna Vilà, from Barcelona University (Spain), for the XPS and EELS analyses performed.  
47  
48  
49  
50  
51  
52

### 53 **References**

- 54  
55  
56  
57 [1] K. Ellmer, A. Klein and B. Rech, *Transparent Conductive Zinc Oxide: Basics and*  
58 *Applications in Thin Film Solar Cells*, Springer, Berlin (2008).  
59 [2] A. L. H.L. Hartnagel, Dawar, A.K. Jain, C Jagadish: , *Semiconducting Transparent Thin*  
60 *Films* Institute of Physics Publishing, Bristol (1995).  
[3] N. Tsuda, K. Nasu, A. Fujimore and K. Siratori, *Electronic Conduction in Oxides*  
Springer-Verlag, Berlin (2000).

1  
2  
3  
4  
5  
6  
7  
8  
9  
10  
11  
12  
13  
14  
15  
16  
17  
18  
19  
20  
21  
22  
23  
24  
25  
26  
27  
28  
29  
30  
31  
32  
33  
34  
35  
36  
37  
38  
39  
40  
41  
42  
43  
44  
45  
46  
47  
48  
49  
50  
51  
52  
53  
54  
55  
56  
57  
58  
59  
60

- [4] P. Canhola, N. Martins, L. Raniero, S. Pereira, E. Fortunato, I. Ferreira and R. Martins, *Thin Solid Films* 487 (2005), p. 271.
- [5] T. Minami, Transparent and conductive multicomponent oxide films prepared by magnetron sputtering, *45th National Symposium of the American-Vacuum-Society*, Baltimore, Maryland (1998).
- [6] I. Baia, B. Fernandes, P. Nunes, M. Quintela and R. Martins, *Thin Solid Films* 383 (2001), p. 244.
- [7] I. Baia, M. Quintela, L. Mendes, P. Nunes and R. Martins, *Thin Solid Films* 337 (1999), p. 171.
- [8] L. Raniero, I. Ferreira, A. Pimentel, A. Goncalves, P. Canhola, E. Fortunato and R. Martins, *Thin Solid Films* 511 (2006), p. 295.
- [9] E. Fortunato, P. Nunes, A. Marques, D. Costa, H. Aguas, I. Ferreira, M. E. V. Costa and R. Martins, *Key Eng. Materials* 230-2 (2002), p. 571.
- [10] P. Nunes, E. Fortunato, P. Tonello, F. B. Fernandes, P. Vilarinho and R. Martins, *VACUUM* 64 (2002), p. 281.
- [11] E. Fortunato, P. Nunes, D. Costa, D. Brida, I. Ferreira and R. Martins, *Vacuum* 64 (2002), p. 233.
- [12] P. Nunes, E. Fortunato, R. Martins and P. Vilarinho, *Key Eng. Materials* 230-2 (2002), p. 424.
- [13] E. Fortunato, P. Nunes, A. Marques, D. Costa, H. Aguas, I. Ferreira, M. E. V. Costa and R. Martins, *Key Eng. Materials* 230-2 (2002), p. 571.
- [14] [www.environmentalchemistry.com](http://www.environmentalchemistry.com).
- [15] V. Assuncao, E. Fortunato, A. Marques, A. Goncalves, I. Ferreira, H. Aguas and R. Martins, *Thin Solid Films* (2003), p. 102.
- [16] E. Fortunato, L. Raniero, L. Silva, A. Goncalves, A. Pimentel, P. Barquinha, H. Aguas, L. Pereira, G. Goncalves, I. Ferreira, E. Elangovan and R. Martins, *Solar Energy Materials and Solar Cells* 92 (2008), p. 1605.
- [17] R. Martins, P. Barquinha, A. Pimentel, L. Pereira and E. Fortunato, *Physica Status Solidi a-Applications and Materials Science* 202 (2005), p. R95.
- [18] R. Martins, P. Barquinha, A. Pimentel, L. Pereira, E. Fortunato, D. Kang, I. Song, C. Kim, J. Park and Y. Park, *Thin Solid Films* 516 (2008), p. 1322.
- [19] H. S. Bae, M. H. Yoon, J. H. Kim and S. Im, *Applied Physics Letters* 83 (2003), p. 5313.
- [20] K. Nomura, H. Ohta, K. Ueda, T. Kamiya, M. Hirano and H. Hosono, *Science* 300 (2003), p. 1269.
- [21] J. F. Wager, *Science* 300 (2003), p. 1245.
- [22] E. Fortunato, A. Pimentel, L. Pereira, A. Goncalves, G. Lavareda, H. Aguas, I. Ferreira, C. N. Carvalho and R. Martins, High field-effect mobility zinc oxide thin film transistors produced at room temperature, *20th International Conference on Amorphous and Microcrystalline Semiconductors*, Campos do Jordao, BRAZIL (2003).
- [23] E. M. C. Fortunato, P. M. C. Barquinha, A. Pimentel, A. M. F. Goncalves, A. J. S. Marques, R. F. P. Martins and L. M. N. Pereira, *Applied Physics Letters* 85 (2004), p. 2541.
- [24] R. Martins, P. Barquinha, L. Pereira, N. Correia, G. Goncalves, I. Ferreira and E. Fortunato, *Applied Physics Letters* 93 (2008).
- [25] E. Fortunato, N. Correia, P. Barquinha, L. Pereira, G. Goncalves and R. Martins, *Ieee Electron Device Letters* 29 (2008), p. 988.
- [26] P. F. Carcia, R. S. McLean and M. H. Reilly, *Journal of the Society for Information Display* 13 (2005), p. 547.
- [27] P. F. Carcia, R. S. McLean and M. H. Reilly, *Applied Physics Letters* 88 (2006).
- [28] P. F. Carcia, R. S. McLean, M. H. Reilly, I. Malajovich, K. G. Sharp, S. Agrawal and G. Nunes, ZnO thin film transistors for flexible electronics, In: N. C. B. R. G. B. E. J. J. Fruehauf,

1  
2  
3 Editor, *Symposium on Flexible Electronics-Materials and Device Technology held at the 2003*  
4 *MRS Spring Meeting*, San Francisco, Ca (2003).

5 [29] R. Martins, E. Fortunato, P. Nunes, I. Ferreira, A. Marques, M. Bender, N. Katsarakis,  
6 V. Cimalla and G. Kiriakidis, *Journal of Applied Physics* 96 (2004), p. 1398.

7 [30] P. Barquinha, L. Pereira, G. Goncalves, R. Martins and F. E., *J. Electrochem. Soc.* 156  
8 (2009), p. H161.

9 [31] P. Barquinha, L. Pereira, G. Goncalves, R. Martins and E. Fortunato, *Electrochemical*  
10 *and Solid State Letters* 11 (2008), p. H248.

11 [32] P. Barquinha, A. Vila, G. Goncalves, L. Pereira, R. Martins, J. Morante and E.  
12 Fortunato, *Physica status solidi a* 205 (2008), p. 1905.

13 [33] P. Barquinha, A. M. Vila, G. Goncalves, R. Martins, J. R. Morante, E. Fortunato and L.  
14 Pereira, *Ieee Transactions on Electron Devices* 55 (2008), p. 954.

15 [34] H. Q. Chiang, B. R. McFarlane, D. Hong, R. E. Presley and J. F. Wager, *Journ. Non-*  
16 *Cryst. Solids* 354 (2008), p. 2826.

17 [35] C. S. Chuang, T. C. Fung, B. G. Mullins, K. Nomura, T. Kamiya, H. P. D. Shieh, H.  
18 Hosono and J. Kanicki, Photosensitivity of amorphous IGZO TFTs for active-matrix flat-panel  
19 displays, *International Symposium of the Society-for-Information-Display (SID 2008)*, Los  
20 Angeles, CA (2008).

21 [36] D. Hong, G. Yerubandi, H. Q. Chiang, M. C. Spiegelberg and J. F. Wager, *Critical*  
22 *Reviews in Solid State and Materials Sciences* 33 (2008), p. 101.

23 [37] M. Noborio, J. Suda and T. Kimoto, *Applied Physics Letters* 93 (2008).

24 [38] H. Ohta, K. Sugiura and K. Koumoto, *Inorganic Chemistry* 47 (2008), p. 8429.

25 [39] D. Look, Donors and acceptors in bulk ZnO grown by the hydrothermal, vapor-phase,  
26 and melt processes, In: J. J. C. L. D. C. Y. T. B. F. Christen, Editor, *Symposium on Zinc Oxide*  
27 *and Related Materials held at the 2006 MRS Fall Meeting*, Boston, MA (2006).

28 [40] N. Tsuboi, T. Hoshino, S. Kobayashi, K. Kato and F. Kaneko, *Physica Status Solidi a-*  
29 *Applications and Materials Science* 203 (2006), p. 2723.

30 [41] K. Nakaoka and K. Ogura, *Journal of the Electrochemical Society* 149 (2002), p. C579.

31 [42] H. Kawazoe, H. Yanagi, K. Ueda and H. Hosono, *Mrs Bulletin* 25 (2000), p. 28.

32 [43] A. Watanabe, *Journal of Solid State Chemistry* 153 (2000), p. 174.

33 [44] A. Kudo, H. Yanagi, K. Ueda, H. Hosono, H. Kawazoe and Y. Yano, *Applied Physics*  
34 *Letters* 75 (1999), p. 2851.

35 [45] H. Kawazoe, M. Yasukawa, H. Hyodo, M. Kurita, H. Yanagi and H. Hosono, *Nature*  
36 389 (1997), p. 939.

37 [46] Y. Ogo, H. Hiramatsu, K. Nomura, H. Yanagi, T. Kamiya, M. Hirano and H. Hosono,  
38 *Applied Physics Letters* 93 (2008).

39 [47] K. W. Böer, *Survey in Semiconductor Physics, Electrons and Other Particles in Bulk*  
40 *Semiconductors*, Van Nostrand Reinhold, New York (1990).

41 [48] R. Martins, P. Barquinha, L. Pereira, I. Ferreira and E. Fortunato, *Applied Physics a-*  
42 *Materials Science & Processing* 89 (2007), p. 37.

43 [49] R. Martins, P. Baptista, L. Raniero, G. Doria, L. Silva, R. Franco and E. Fortunato,  
44 *Applied Physics Letters* 90 (2007).

45 [50] M. Shur, *Physics of Semiconductor Devices* Prentice Hill, New Jersey, USA (1990).

46 [51] R. A. Street, *Technology and Applications of Amorphous Semiconductors*, Springer,  
47 Berlin (2000).

48 [52] J. Robertson, *Physica Status Solidi B-Basic Solid State Physics* 245 (2008), p. 1026.

49 [53] H. Hosono, K. Nomura, Y. Ogo, T. Uruga and T. Kamiya, Factors controlling electron  
50 transport properties in transparent amorphous oxide semiconductors, *22nd International*  
51 *Conference on Amorphous and Nanocrystalline Semiconductors*, Breckenridge, CO (2007).

52 [54] R. Martins, P. Barquinha, I. Ferreira, L. Pereira, G. Goncalves and E. Fortunato, *Journal*  
53 *of Applied Physics* 101 (2007).

1  
2  
3  
4  
5  
6  
7  
8  
9  
10  
11  
12  
13  
14  
15  
16  
17  
18  
19  
20  
21  
22  
23  
24  
25  
26  
27  
28  
29  
30  
31  
32  
33  
34  
35  
36  
37  
38  
39  
40  
41  
42  
43  
44  
45  
46  
47  
48  
49  
50  
51  
52  
53  
54  
55  
56  
57  
58  
59  
60

- [55] W. E. Spear and P. G. Lecomber, *Solid State Communications* 17 (1975), p. 1193.
- [56] P. G. Lecomber, W. E. Spear and A. Ghaith, *Electronics Letters* 15 (1979), p. 179.
- [57] T. Tsukada, *Active-Matrix Liquid-Crystal Displays*, in *The Technology and applications of amorphous silicon*, R. A. Street, ed., Springer Verlagen, 2000, p. 7.
- [58] A. J. Snell, K. D. Mackenzie, W. E. Spear, P. G. Lecomber and A. J. Hughes, *Applied Physics* 24 (1981), p. 357.
- [59] H. Hosono, M. Yasukawa and H. Kawazoe, *Journal of Non-Cryst. Solids* 203 (1996), p. 334.
- [60] E. M. C. Fortunato, L. M. N. Pereira, P. M. C. Barquinha, A. M. B. do Rego, G. Goncalves, A. Vila, J. R. Morante and R. F. P. Martins, *Applied Physics Letters* 92 (2008).
- [61] E. Fortunato, P. Barquinha, A. Pimentel, L. Pereira, G. Goncalves and R. Martins, *Physica Status Solidi-Rapid Research Letters* 1 (2007), p. R34.
- [62] R. Martins, P. Almeida, P. Barquinha, L. Pereira, A. Pimentel, I. Ferreira and E. Fortunato, *Journal of non-Cryst. Solids* 352 (2006), p. 1471.
- [63] L. Pereira, H. Aguas, M. Beckers, R. M. S. Martins, E. Fortunato and R. Martins, *J. Non-crystalline Solids* 352 (2006), p. 1204.
- [64] L. Pereira, P. Barquinha, E. Fortunato and R. Martins, *J. Non-crystalline Solids* 354 (2008), p. 2534.
- [65] L. Pereira, P. Barquinha, E. Fortunato, R. Martins, D. Kang, C. J. Kim, H. Lim, I. Song and Y. Park, *Thin Solid Films* (2008), p. 1544.
- [66] H. Aguas, N. Popovici, L. Pereira, O. Conde, W. R. Branford, L. F. Cohen, E. Fortunato and R. Martins, *Physica Status Solidi a-Applications and Materials Science* 205 (2008), p. 880.
- [67] R. Martins, H. Aguas, I. Ferreira, E. Fortunato, S. Lebib, P. R. I. Cabarocas and L. Guimaraes, *Chemical Vapor Deposition* 9 (2003), p. 333.
- [68] D. Kang, I. Song, C. Kim, Y. Park, T. D. Kang, H. S. Lee, J. W. Park, S. H. Baek, S. H. Choi and H. Lee, *Applied Physics Letters* 91 (2007).
- [69] H. Hosono, K. Nomura, Y. Ogo, T. Uruga and T. Kamiya, *J. Non-Cryst. Solids* 354 (2008), p. 2796.
- [70] M. R. Vilar, J. El Beghdadi, F. Debontridder, R. Artzi, R. Naaman, A. M. Ferraria and A. M. B. do Rego, *Surface and Interface Analysis* 37 (2005), p. 673.
- [71] V. M. Jimenez, J. A. Mejias, J. P. Espinos and A. R. GonzalezElipe, *Surface Science* 366 (1996), p. 545.
- [72] J. C. Manificier and L. Szepessy, *Applied Physics Letters* 31 (1977), p. 459.
- [73] T. Feng, A. K. Ghosh and C. Fishman, *Journal of Applied Physics* 50 (1979), p. 4972.
- [74] J. B. Dubow, D. E. Burk and J. R. Sites, *Applied Physics Letters* 29 (1976), p. 494.
- [75] H. Kobayashi, H. Mori, T. Ishida and Y. Nakato, *Journal of Applied Physics* 77 (1995), p. 1301.
- [76] H. Q. Chiang, J. F. Wager, R. L. Hoffman, J. Jeong and D. A. Keszler, *Applied Physics Letters* 86 (2005).
- [77] V. Figueiredo, E. Elangovan, G. Goncalves, P. Barquinha, L. Pereira, N. Franco, E. Alves, R. Martins and E. Fortunato, *Applied Surface Science* 254 (2008), p. 3949.
- [78] <http://www.oled.info.com/samsung-electronics-developed-new-amorphous-oxide-tft>, *World's Largest 40" OLED*, Engadgetd (2009).

## Figure Captions

Fig. 1. (color online) a) A view of the apparatus and the clean room where the oxide materials and the devices were processed; b) a sketch of the co-sputtering process, allowing to analyze in the same run changes in the films' composition (film close to the right side is Sn rich, while the opposite occurs on the left side); c) electrical testing structures used to determine the films' conductivity as a function of temperature and for hall effect measurements.

Fig. 2. (color online) XRD patterns of the a-IZO, poly-ZnO and poly-ZGO films. The labels indicate the film thickness and oxygen partial pressure used. The images on the left and right sides were obtained by AFM and SEM analysis, respectively.

Fig. 3. (color online) a) XRD patterns of the a-ZGSO deposited at R.T. on a glass substrate, before and after annealing at 300 °C; b) SEM cross section of the ZGSO film deposited on a c-Si substrate coated with a thin SiO<sub>2</sub> layer, c) SEM surface image of the ZGSO film; d) AFM surface image of the same ZGSO film; e) SEM cross section of the p-c-Si/a-IZO/ZGO solar cell.

Fig. 4.a) Comparison of the refractive index (n) and the extinction coefficient (k) spectra of ZGO and ZGSO films obtained by spectroscopic ellipsometry; b) Arrhenius plot of the conductivity of a-ZGSO films with different Sn contents.

Fig. 5. I-V curves of the produced solar cells under AM1.5 illumination: a) p-c-Si/poly-ZGO; b) p-c-Si/a-IZO/poly-ZGO.

1  
2  
3  
4 Fig. 6. Transfer and output characteristics of TFTs based on ZnO produced at R.T and a-  
5  
6 ZGSO produced at 150 °C: a) transfer characteristics for ZnO TFTs annealed at 150 and  
7  
8 300 °C; b) output characteristics for ZnO TFTs annealed at 150 °C; c) transfer  
9  
10 characteristics for ZGSO TFTs annealed at 250 and 300 °C; output characteristics for  
11  
12 ZGSO TFTs annealed at 200 °C.  
13  
14  
15  
16  
17  
18  
19

20 Fig. 7. Electrical performance of the ZCO TFT processed at 150 °C and annealed at 350 °C:  
21  
22 a) transfer and b) output characteristics.  
23  
24  
25  
26  
27  
28  
29  
30  
31  
32  
33  
34  
35  
36  
37  
38  
39  
40  
41  
42  
43  
44  
45  
46  
47  
48  
49  
50  
51  
52  
53  
54  
55  
56  
57  
58  
59  
60

## TABLES

Table 1. XPS atomic percentages for Ga, Zn, Sn and O elements and Ga/Zn and Sn/Zn atomic ratios

<i>Annealing temperature</i>	<i>Ga</i>	<i>Zn</i>	<i>Sn</i>	<i>O</i> (Oxide)	<i>O</i> (Hydroxide)	<i>Ga/Zn</i>	<i>Sn/Zn</i>
RT	1.6	24.6	6.6	35.5	31.7	0.07	0.27
200°C	1.6	24.6	7.2	40.4	26.2	0.07	0.29
300°C	2.5	21.2	11.8	45.5	19.2	0.12	0.56

Table 2. Electrical characteristics of the ZnO, ZGO and ZGSO films processed under different deposition conditions, before and after annealing.

<i>Sample/ target side</i>	<i>Resistivity (<math>\Omega\text{cm}</math>)</i>	<i>Carrier mobility (<math>\text{cm}^2\text{V}^{-1}\text{s}^{-1}</math>)</i>	<i>Carrier concentration (<math>\text{cm}^{-3}</math>)</i>
poly-ZnO (a)	$1.9 \times 10^5$	--	--
poly-ZnO (b)	$3.1 \times 10^2$	--	--
poly-ZGO (a)	$(2-6) \times 10^{-4}$	10-18.5	$(1.65-9.85) \times 10^{20}$
ZGSO/Sn (a)	$1.5 \times 10^{10}$	--	--
ZGSO/Sn (b)	$9.4 \times 10^1$	5.5	$1.2 \times 10^{16}$
ZGSO/ZGO (a)	$8 \times 10^{10}$	--	--
ZGSO/ZGO (b)	$5.2 \times 10^1$	4.7	$3.1 \times 10^{16}$

(a) as deposited; (b) after annealing at 300 °C.

Table 3- Performance of the pn heterojunction solar cells analysed.

<i>Device type</i>	$J_{sc}$ (mA/cm <sup>2</sup> )	$V_{oc}$ (mV)	$FF$	$\eta$ (%)	<i>Area</i> (cm <sup>2</sup> )
(a) p-Sic/n-poly-ZGO	31.15	488.8	0.59	9.02	2.03
(b) p-Sic/a-IZO/n-polyZGO	31.88	558.8	0.79	14.09	2.34

For Peer Review Only

Table 4. Electrical characteristics of the a-ZGSO and poly-ZnO TFTs, as processed and after annealing.

Annealing (°C)	<i>a-ZGSO S1 (R.T.)</i>				<i>a-ZGSO S2 (150 °C)</i>				<i>Poly-ZnO (R.T.)</i>	
	a)	200	250	300	a)	200	250	300	150	300
$\mu_{SAT}$ (cm <sup>2</sup> /Vs)	nw	nw	7.9	18.1	ns	10.6	15.4	24.6	1.1*	3.5*
$V_T$ (V)	nw	nw	6.5	6.5	ns	5.4	4.8	4.6	9.1	≈-3.3
$I_{ON}/I_{OFF}$	nw	nw	2×10 <sup>7</sup>	6×10 <sup>7</sup>	ns	3×10 <sup>8</sup>	8×10 <sup>7</sup>	8×10 <sup>7</sup>	7×10 <sup>6</sup>	>5×10 <sup>3</sup>
$S$ (V/decade)	nw	nw	0.75	0.62	ns	0.38	0.46	0.45	0.88	--

*a) as-deposited; nw – not working; ns – not stable; \* non-saturated value ( $V_G=30$  V)*

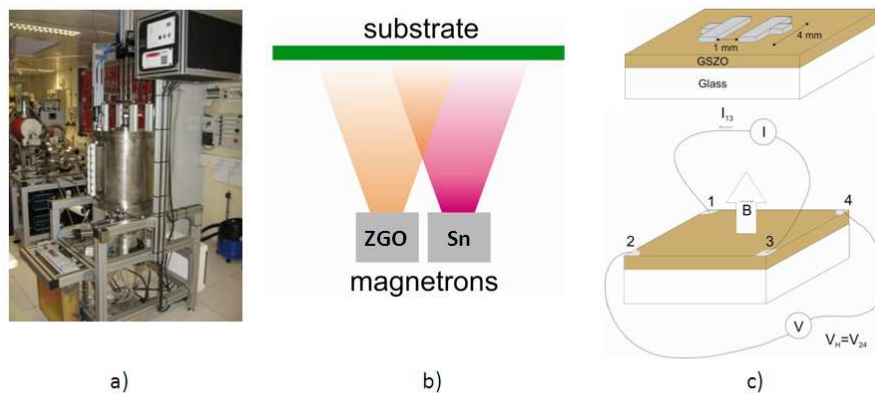


Fig. 1. a) A view of the apparatus and the clean room where the oxide materials and the devices were processed; b) a sketch of the co-sputtering process, allowing to analyze in the same run changes in the films' composition (film close to the right size is Sn rich, while the opposite occurs on the left side); c) electrical testing structures used to determine the films' conductivity as a function of temperature and for hall effect measurements.

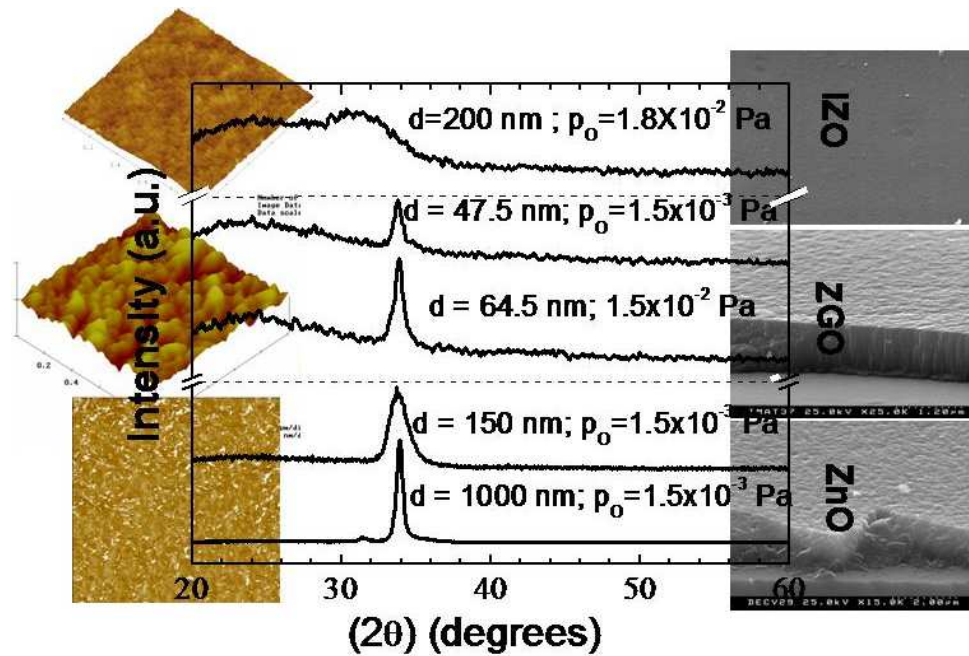


Fig. 2. XRD patterns of the a-IZO, poly-ZnO and poly-ZGO films. The labels indicate the film thickness and oxygen partial pressure used. The images on the left and right sides were obtained by AFM and SEM analysis, respectively.  
207x136mm (96 x 96 DPI)

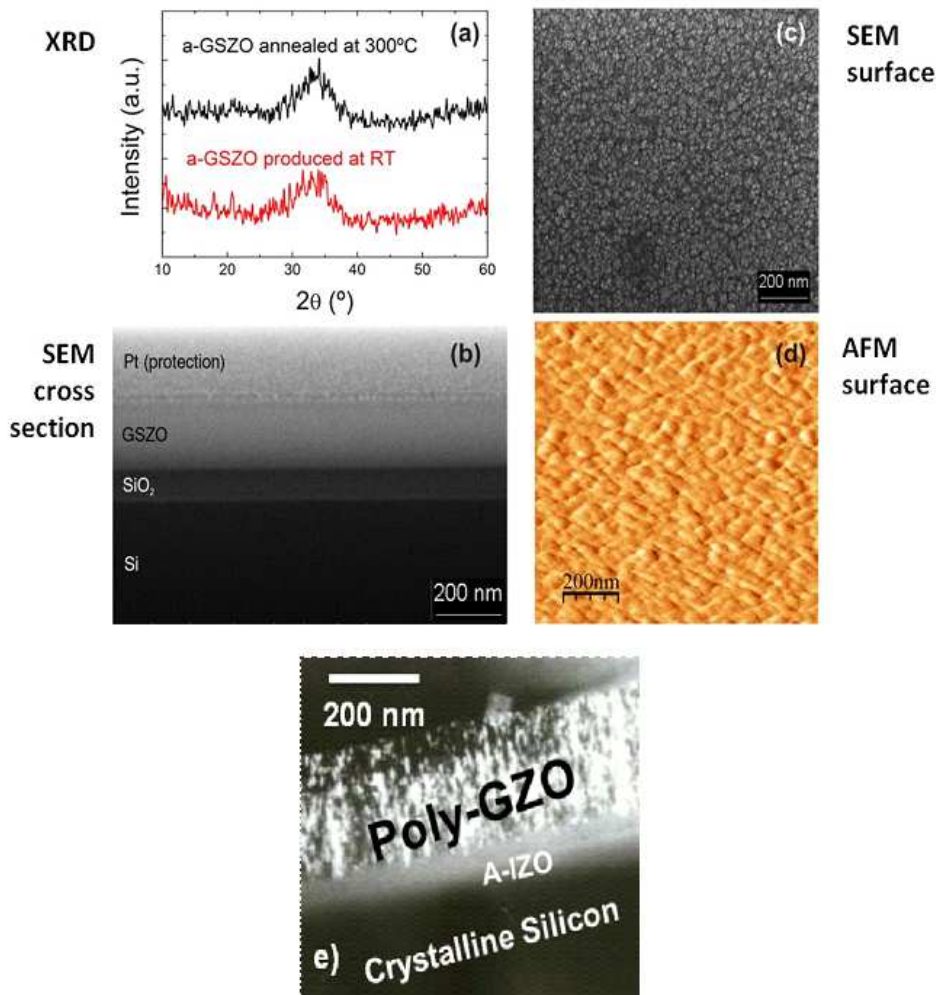
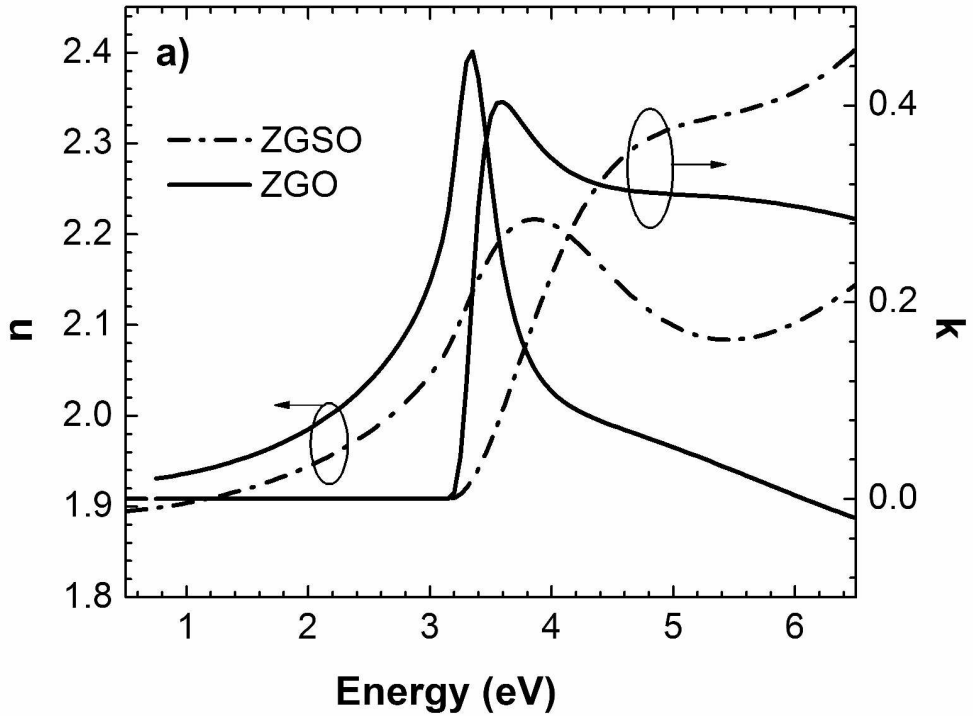


Fig. 3.a) XRD patterns of the a-ZGSZO deposited at R.T. on a glass substrate, before and after annealing at 300 °C; b) SEM cross section of the ZGSZO film deposited on a c-Si substrate coated with a thin SiO<sub>2</sub> layer, c) SEM surface image of the ZGSZO film; d) AFM surface image of the same ZGSZO film; e) SEM cross section of the p-c-Si/a-IZO/ZGO solar cell.

182x194mm (96 x 96 DPI)

1  
2  
3  
4  
5  
6  
7  
8  
9  
10  
11  
12  
13  
14  
15  
16  
17  
18  
19  
20  
21  
22  
23  
24  
25  
26  
27  
28  
29  
30  
31  
32  
33  
34  
35  
36  
37  
38  
39  
40  
41  
42  
43  
44  
45  
46  
47  
48  
49  
50  
51  
52  
53  
54  
55  
56  
57  
58  
59  
60



269x206mm (300 x 300 DPI)

Pre-proof Only

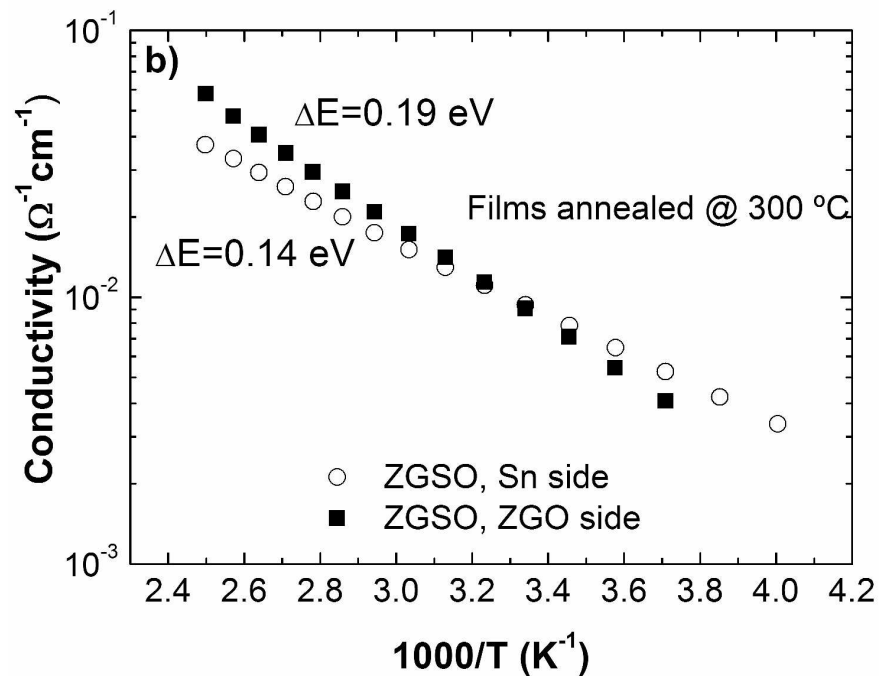


Fig. 4.a) Comparison of the refractive index ( $n$ ) and the extinction coefficient ( $k$ ) spectra of ZGO and ZGSO films obtained by spectroscopic ellipsometry; b) Arrhenius plot of the conductivity of a-ZGSO films with different Sn contents.  
286x201mm (300 x 300 DPI)

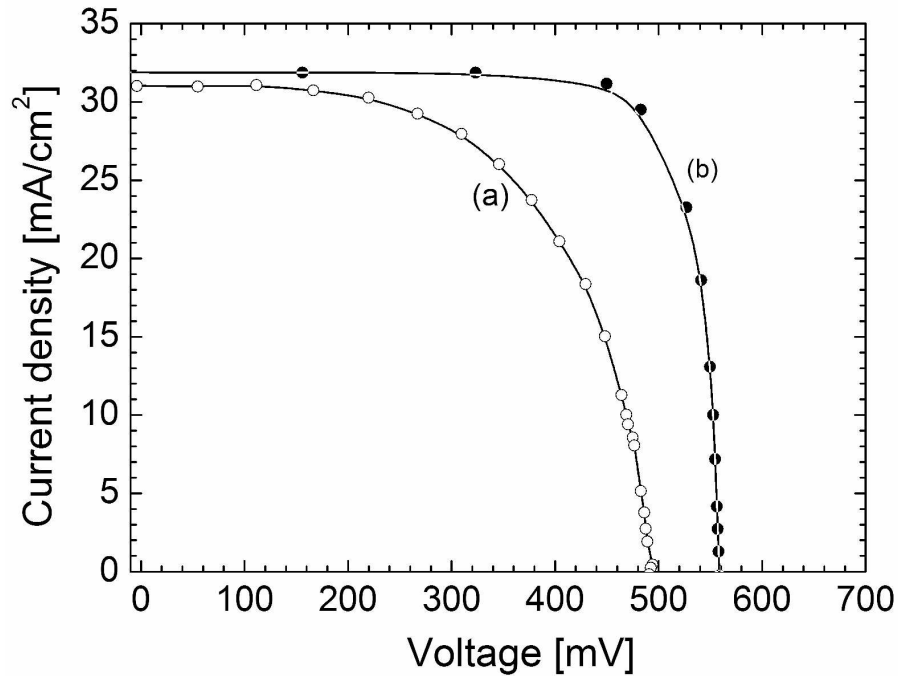
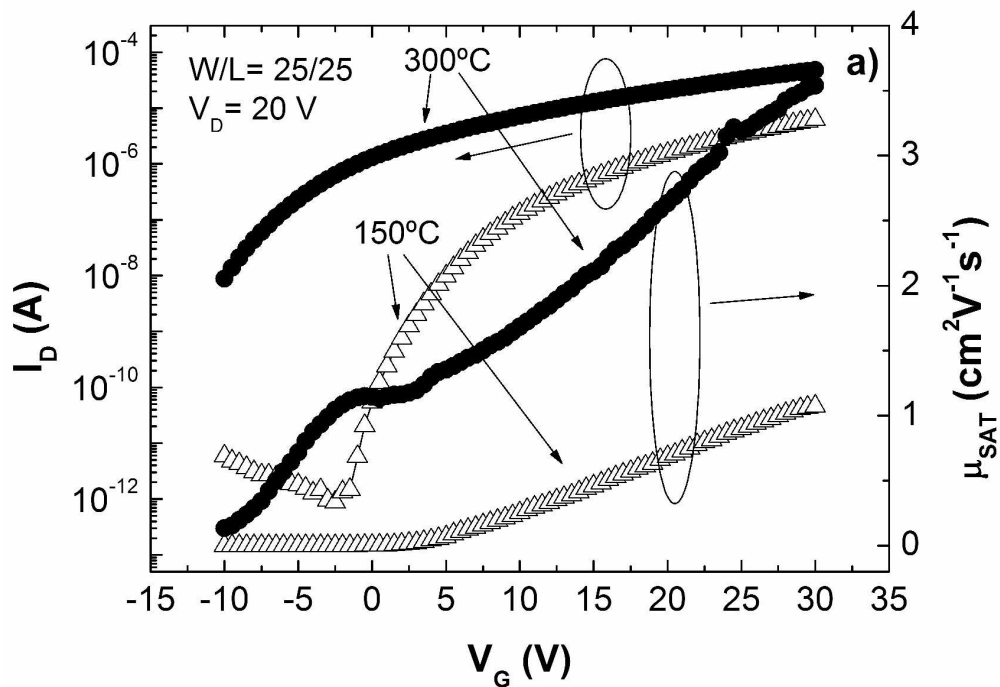
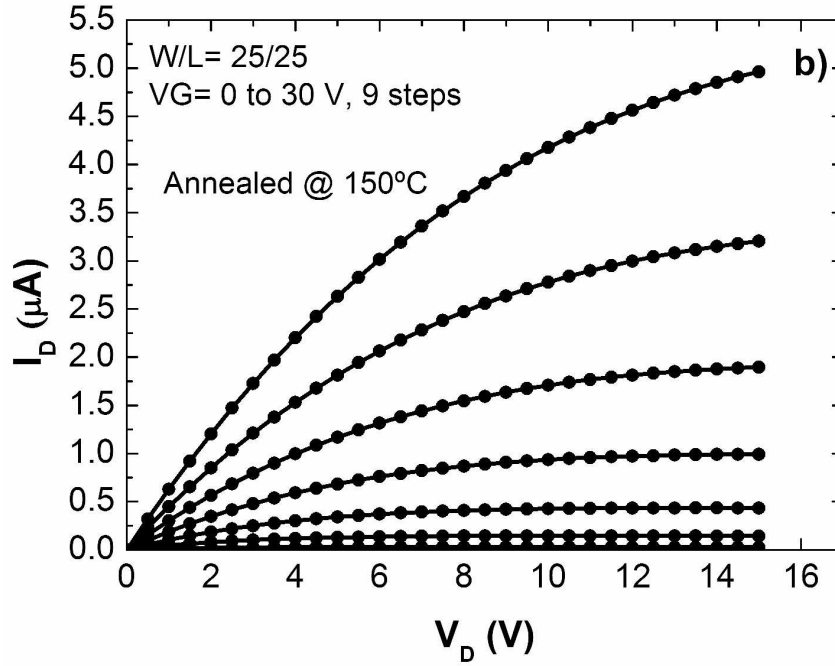


Fig. 5. I-V curves of the produced solar cells under AM1.5 illumination: a) p-c-Si/poly-ZGO; b) p-c-Si/a-IZO/poly-ZGO.  
297x209mm (300 x 300 DPI)



287x201mm (300 x 300 DPI)

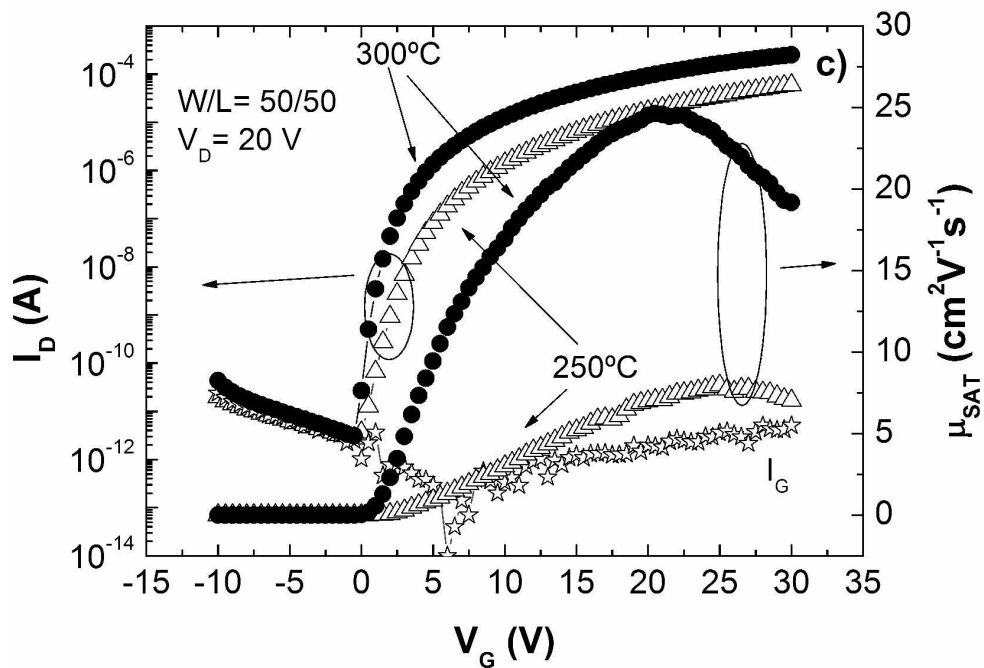
1  
2  
3  
4  
5  
6  
7  
8  
9  
10  
11  
12  
13  
14  
15  
16  
17  
18  
19  
20  
21  
22  
23  
24  
25  
26  
27  
28  
29  
30  
31  
32  
33  
34  
35  
36  
37  
38  
39  
40  
41  
42  
43  
44  
45  
46  
47  
48  
49  
50  
51  
52  
53  
54  
55  
56  
57  
58  
59  
60



286x201mm (300 x 300 DPI)

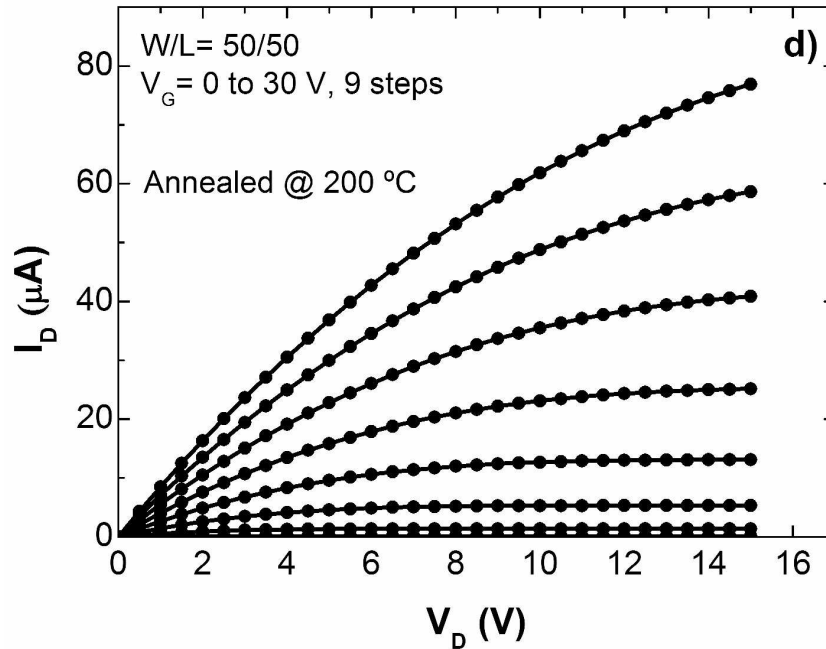
View Only

1  
2  
3  
4  
5  
6  
7  
8  
9  
10  
11  
12  
13  
14  
15  
16  
17  
18  
19  
20  
21  
22  
23  
24  
25  
26  
27  
28  
29  
30  
31  
32  
33  
34  
35  
36  
37  
38  
39  
40  
41  
42  
43  
44  
45  
46  
47  
48  
49  
50  
51  
52  
53  
54  
55  
56  
57  
58  
59  
60



286x201mm (300 x 300 DPI)

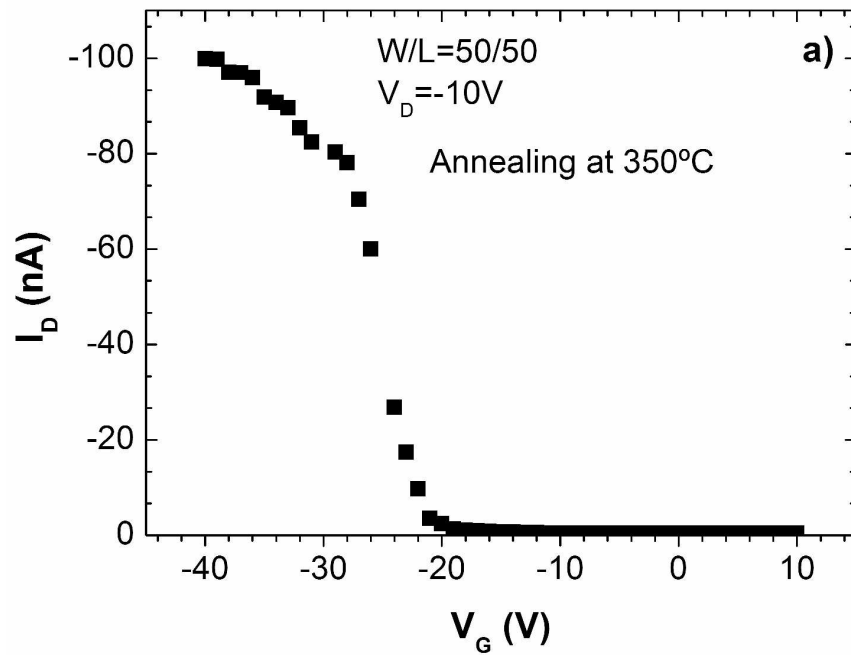
1  
2  
3  
4  
5  
6  
7  
8  
9  
10  
11  
12  
13  
14  
15  
16  
17  
18  
19  
20  
21  
22  
23  
24  
25  
26  
27  
28  
29  
30  
31  
32  
33  
34  
35  
36  
37  
38  
39  
40  
41  
42  
43  
44  
45  
46  
47  
48  
49  
50  
51  
52  
53  
54  
55  
56  
57  
58  
59  
60



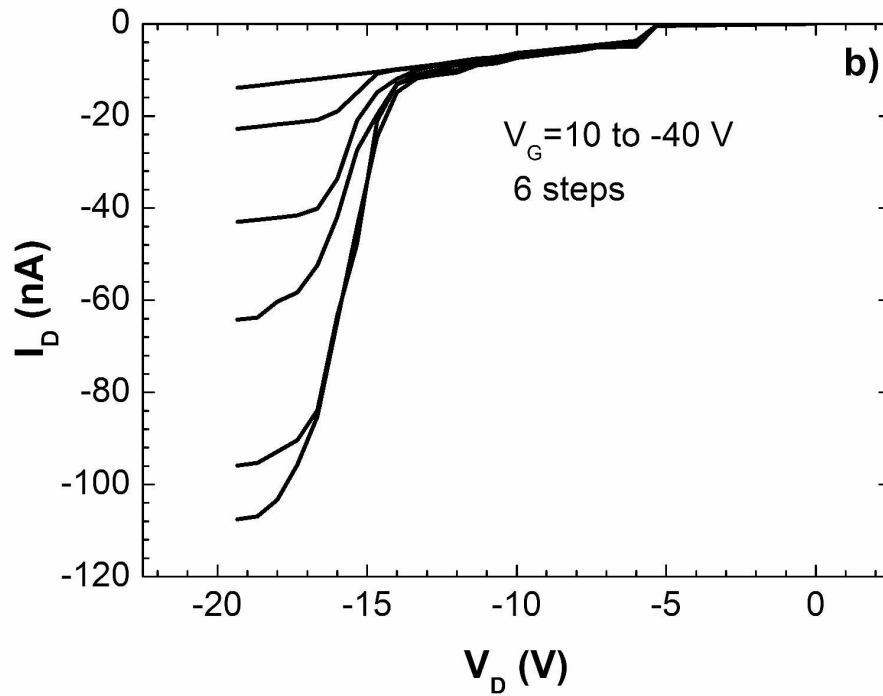
32 Fig. 6. Transfer and output characteristics of TFTs based on ZnO produced at R.T and a-ZGSO  
33 produced at 150 °C: a) transfer characteristics for ZnO TFTs annealed at 150 and 300 °C; b) output  
34 characteristics for ZnO TFTs annealed at 150 °C; c) transfer characteristics for ZGSO TFTs annealed  
35 at 250 and 300 °C; output characteristics for ZGSO TFTs annealed at 200 °C.

286x201mm (300 x 300 DPI)

36  
37  
38  
39  
40  
41  
42  
43  
44  
45  
46  
47  
48  
49  
50  
51  
52  
53  
54  
55  
56  
57  
58  
59  
60



286x201mm (300 x 300 DPI)



32 Fig. 7. Electrical performance of the ZCO TFT processed at 150  $\mu$ C and annealed at 350  $^{\circ}$ C: a)  
33 transfer and b) output characteristics.  
34 286x201mm (300 x 300 DPI)

35  
36  
37  
38  
39  
40  
41  
42  
43  
44  
45  
46  
47  
48  
49  
50  
51  
52  
53  
54  
55  
56  
57  
58  
59  
60